

DOI: 10.1002/cbic.200800096

# Exploring the Conserved Water Site and Hydration of a Coiled-Coil Trimerisation Motif: A MD Simulation Study

Jožica Dolenc,<sup>[a, b]</sup> Riccardo Baron,<sup>[a]</sup> John H. Missimer,<sup>[c]</sup> Michel O. Steinmetz,<sup>[c]</sup> and Wilfred F. van Gunsteren<sup>\*[a]</sup>

*The solvent structure and dynamics around ccβ-p, a 17-residue peptide that forms a parallel three-stranded α-helical coiled coil in solution, was analysed through 10 ns explicit solvent molecular dynamics (MD) simulations at 278 and 330 K. Comparison with two corresponding simulations of the monomeric form of ccβ-p was used to investigate the changes of hydration upon coiled-coil formation. Pronounced peaks in the solvent density distribution between residues Arg8 and Glu13 of neighbouring helices show the presence of water bridges between the helices of the ccβ-p trimer; this is in agreement with the water sites observed in X-ray crystallography experiments. Interestingly, this water site is structurally conserved in many three-stranded coiled coils and,*

*together with the Arg and Glu residues, forms part of a motif that determines three-stranded coiled-coil formation. Our findings show that little direct correlation exists between the solvent density distribution and the temporal ordering of water around the trimeric coiled coil. The MD-calculated effective residence times of up to 40 ps show rapid exchange of surface water molecules with the bulk phase, and indicate that the solvent distribution around biomolecules requires interpretation in terms of continuous density distributions rather than in terms of discrete molecules of water. Together, our study contributes to understanding the principles of three-stranded coiled-coil formation.*

## Introduction

Water plays a crucial role in determining the structure of biological macromolecules, because the thermodynamics and dynamics of water and biomolecules are tightly coupled.<sup>[1–3]</sup> Different dynamical behaviour can be distinguished for water molecules that are buried in cavities or surface clefts in the interior of a macromolecule, for hydration water that interacts with the surfaces of macromolecules, which is more mobile than internal water, or for bulk water.<sup>[4–6]</sup> Therefore, understanding the hydration of macromolecules requires an atomic-level structural and dynamical description of the system of interest.

A variety of experimental techniques such as X-ray and neutron diffraction<sup>[7–11]</sup> and NMR spectroscopy<sup>[11–15]</sup> have been employed successfully to investigate the hydration of biological macromolecules. However, experiments provide only temporal or ensemble averages<sup>[6, 8, 16–18]</sup> and for technical reasons may be carried out on samples that are in other physicochemical environments than the biologically relevant one; this makes the interpretation of the results nontrivial.<sup>[7, 10, 11, 19, 20]</sup> On the other hand, computer simulations are able to provide an atomistic description of the system that includes the temporal and ensemble distributions of both solute and solvent.<sup>[6, 19, 21–33]</sup>

Here, we investigate the hydration behaviour of the de-novo-designed 17-residue ccβ-p peptide with the amino acid sequence S-IRELEAR-IRELELR-IG which forms a parallel three-stranded α-helical coiled coil in solution<sup>[34–36]</sup> by using explicit solvent molecular dynamics simulations at two temperatures, 278 and 330 K. The structure of the ccβ-p trimer has been solved to high resolution by X-ray crystallography.<sup>[34]</sup> A prominent feature of the three-stranded coiled coil is a bifurcated

salt-bridge contact formed between Arg8:Nε,Nη2 of one chain and Glu13:Oε1,Oε2 of the neighbouring chain (Figure 1). A water-mediated hydrogen bond between Arg8:O and Glu13:Oε2 completes this network. Remarkably, this distinct motif, including the position of the crystallographic water site, as illustrated in Figure 1, is conserved in many three-stranded coiled-coil domains of intracellular, extracellular, viral, and synthetic proteins.<sup>[37]</sup> Mutation of Arg8 resulted in a change of the oligomerisation state;<sup>[36]</sup> this further supports the importance of the characteristic electrostatic interactions and the bridging water molecule for determining the trimeric ccβ-p coiled-coil structural stability. The contribution to protein stability that is provided by these salt-bridge networks has been recently investigated by MD simulations in explicit water and analysis of configurational entropy.<sup>[38]</sup>

In the present analysis, we explore the role of the conserved water site in the trimerisation motif by characterising both the spatial and temporal ordering of the water molecules around

[a] Dr. J. Dolenc, Dr. R. Baron, Prof. Dr. W. F. van Gunsteren  
Laboratory of Physical Chemistry, Swiss Federal Institute of Technology  
8093 Zürich (Switzerland)  
Fax: (+41) 44-632-10-39  
E-mail: wfvgn@igc.phys.chem.ethz.ch

[b] Dr. J. Dolenc  
Faculty of Chemistry and Chemical Technology, University of Ljubljana  
1000 Ljubljana (Slovenia)

[c] Dr. J. H. Missimer, Dr. M. O. Steinmetz  
Biomolecular Research, Structural Biology, Paul Scherrer Institut  
5232 Villigen (Switzerland)

Supporting information for this article is available on the WWW under <http://www.chembiochem.org> or from the author.

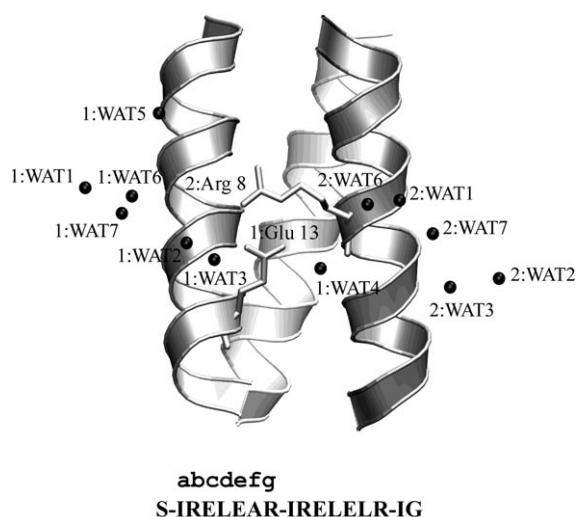


**Figure 1.** The  $cc\beta$ -p coiled coil including the crystallographic water sites that correspond to helices 1 and 2. The amino acid sequence, including the heptad repeats (abcdefg), is indicated, and the trimerisation motif is underlined. The peptide backbones are represented as ribbons. The Arg8 and Glu13 side chains of neighbouring helices 1 and 2 that form an interhelical network with the conserved water site WAT4 are shown in stick representation. The spheres show the location of water oxygen atoms and their designations as in Table 1.

the  $cc\beta$ -p coiled coil in terms of solvent spatial probability distributions, hydrogen bonding, solvent accessibility, water exchange and residence times. We focus on the identification of the regions with the highest solvent probability density and their relation to the water sites that are observed in a high-resolution X-ray study.<sup>[34]</sup>

## Results and Discussion

### Solvent density distribution

In Figure 2, the position of the conserved hydration site WAT4 between the Arg8 and Glu13 residues of the neighbouring helices of the  $cc\beta$ -p trimer is compared with the peaks in the solvent density distribution derived from the MD simulations at 278 and 330 K. The number density distribution of the water oxygen in Figure 2 corresponds to 2.5 times the bulk water density (that is,  $83.6 \text{ nm}^{-3}$ ). The results show that the water site, WAT4, that is close to Arg8 and Glu13, which is the highly conserved structural motif appears between all helix pairs of the  $cc\beta$ -p trimer at both temperatures. The pattern becomes particularly clear at higher temperature; this indicates 1) better sampling of the (solvent) configurational space at 330 K and 2) a reduction of solvent-shielding effects with increased temperature.<sup>[38,39]</sup>

Regarding the additional water sites reported in the X-ray crystal structure of the  $cc\beta$ -p coiled coil, a maximum of two times the bulk water number density (that is,  $66.9 \text{ nm}^{-3}$ ) has been observed at 278 K for water site WAT7, which is located close to the  $C\delta$  atom of Glu11 and carbonyl oxygen of Ala7. At 330 K two weak maxima in the number density distribution have been found in the vicinity of the crystallographic water sites WAT3 and WAT7. On the other hand, the crystallographic water sites WAT1, WAT2 and WAT5 do not stand out as hydration sites in the solvent density distribution, which suggests that the water molecules are trapped at the specified positions because of crystal packing effects. A detailed analysis of the crystal structure reveals that the water molecule that corresponds to the site WAT1 is hydrogen bonded to water molecule WAT6. Similarly, the water molecule that occupies water site WAT2 is hydrogen bonded to the water molecule that corresponds to site WAT3 (Table 1).

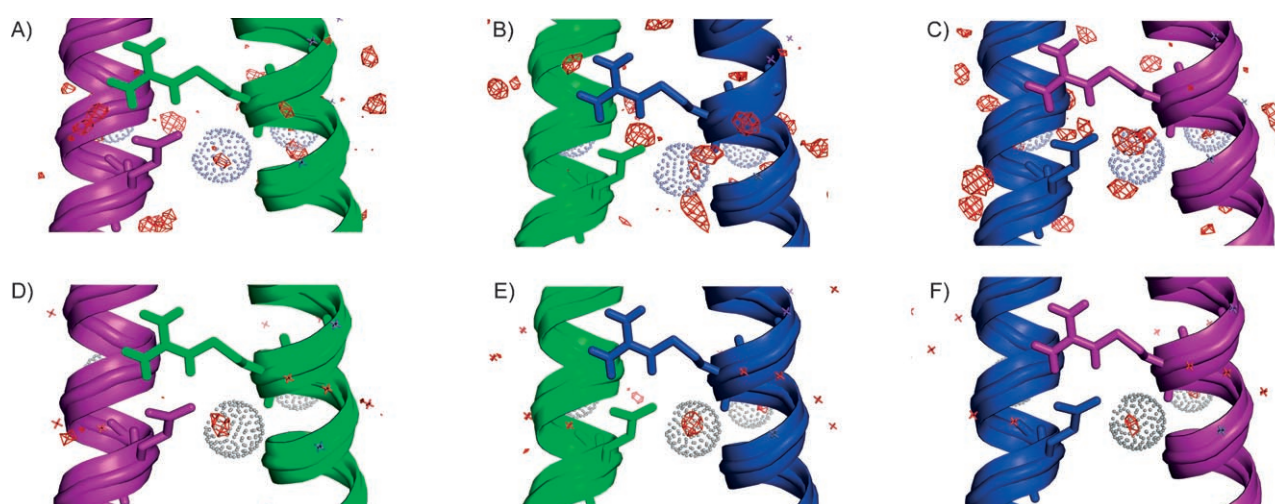


**Figure 2.** Comparison of the position of the conserved crystallographic water site WAT4 (dotted sphere) with the peaks in three-dimensional solvent (oxygen) number density distribution around the  $cc\beta$ -p coiled coil (red contours) at 278 K (upper panels) and at 330 K (lower panels). Each of the three helices is coloured distinctly (helix 1 in purple, helix 2 in green, helix 3 in blue) and the side chains of Arg8 and Glu13 of the neighbouring helices are shown in stick representation. The contour threshold corresponds to 2.5 times the bulk water density.

Table 1. Designations of crystallographic water sites and their distances ( <i>d</i> ) from nearest residue side chains and water sites for the ccβ-p coiled coil.					
Water site	Location	<i>d</i> [nm]	Water site	Location	<i>d</i> [nm]
1:WAT1	1 GLU4:Cδ	0.46	1:WAT4	1 Glu13:Cδ	0.35
	1 GLU11:Cδ	0.45		3 Arg8:O	0.30
	1 WAT6:O	0.30		1:WAT5	1 Glu7:Cδ
1:WAT2	1 Arg10:Cδ	0.46	1 Arg4:O	0.32	
	1 Leu14:Cγ	0.49	1:WAT6	1 Arg8:Cγ	0.33
	1 WAT3:O	0.31	1 Glu11:Cδ	0.36	
1:WAT3	1 Arg10:O	0.35	1 WAT1:O	0.30	
	1 Glu13:Cδ	0.36	1 Glu11:Cδ	0.31	
	1 WAT2:O	0.31	1 Ala7:O	0.31	

In order to clarify the structural role of water in the conserved water site between the Arg8 and Glu13 residues, the number density distribution for water hydrogen atoms has been calculated and superimposed on the water oxygen density maps (Figure 3). Although the maxima in the number density distribution of the water hydrogen atoms are less well-defined as in case of the water oxygen distribution due to the rotational movements of the water molecules<sup>[40]</sup> (Figure 3), the water hydrogens appear to be oriented with respect to the carbonyl of Arg8 and the side chain of Glu13. Particularly the density distribution between helices 2 and 3 at 330 K clearly shows a water molecule bridging the two helices. As in the case of the water oxygen atoms, the maxima in the number density distribution of hydrogen atoms are more distinct at the higher temperature.

#### Solvent-accessible surface area

The solvent-accessible surface area (SASA) for the ccβ-p monomer and the ccβ-p coiled coil at 278 and 330 K, is displayed in

Figure S1 in the Supporting Information. The SASA time series for the helices 1, 2 and 3 of the ccβ-p coiled coil at 278 and 330 K are shown in the lower three panels, the time series for the monomer is shown in the upper panel. The average areas for the three helices of the trimer at the two temperatures are indistinguishable within the standard deviations; the values are 20.6(±0.5) and 21.1(±0.6) nm<sup>2</sup>, 21.2(±0.6) and 20.9(±0.7) nm<sup>2</sup>, 21.8(±0.7) and 20.9(±0.7) nm<sup>2</sup>, respectively. The similarity among the helices suggests that the simulations have converged well. The similarity between temperatures confirms the stability of the ccβ-p coiled coil in both molecular dynamics simulations. Averages and standard deviations are about half those of the monomer at the two temperatures: 41.0(±1.2) and 41.6(±1.4) nm<sup>2</sup>; this reflects the inaccessibility of the trimer interior to solvent. In other words, about 48% and 50% of water molecules (at 278 and 330 K, respectively) vacate the peptide surface when three ccβ-p heptadecamer strands form the coiled-coil trimer. This reflects the tight packing of the trimer that is produced by salt-bridge networks between the neighbouring chains and by the presence of several hydrophobic contacts between the strands of the ccβ-p coiled coil.

#### Solute-solvent hydrogen bonding

Figure 4 displays the solute-solvent hydrogen bonds for the ccβ-p monomer and the ccβ-p trimer at 278 and 330 K. The Oε1 and Oε2 side-chain atoms of the Glu residues exhibit strong hydrogen bonding; the average number of hydrogen bonds,  $\langle N_{\text{HB}} \rangle$ , ranges from 1.46 in the case of the Glu4 Oε1 atom of the ccβ-p monomer at 330 K to 3.43 in the case of the Glu11 Oε2 atom of the ccβ-p helix 3 at 278 K. In addition to the two-centred hydrogen bonds, three-centred hydrogen bonds between water and the Oε1 and Oε2 atoms of the Glu side chains were observed. Equally important for binding water to the surface of both ccβ-p monomer and ccβ-p trimer

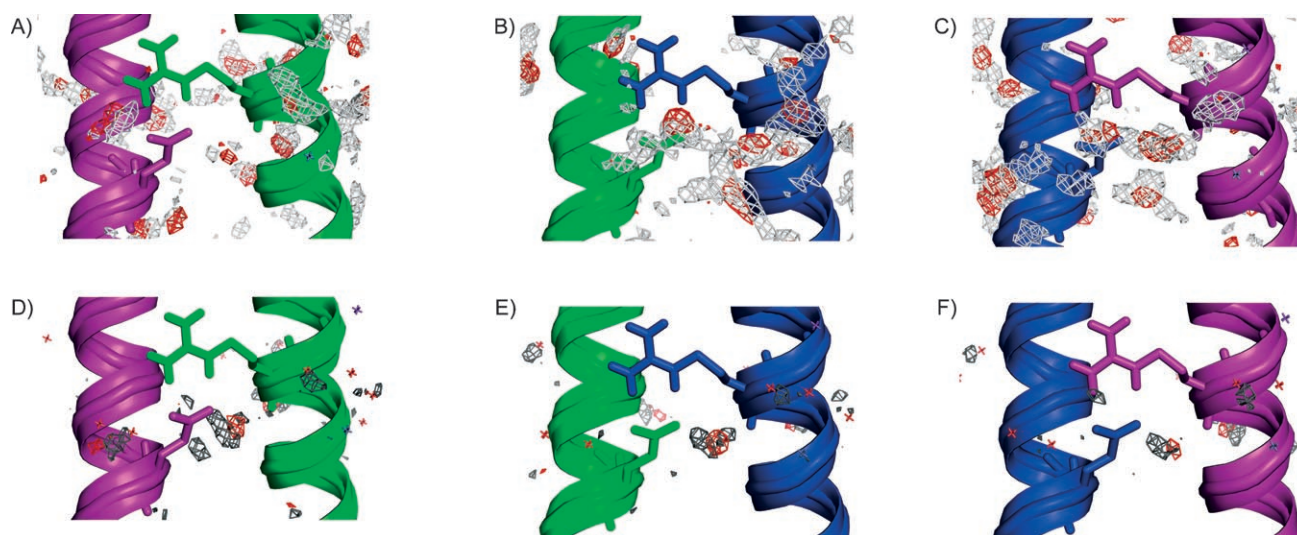


**Figure 3.** Number density distribution for water oxygens (red contours) and hydrogens (grey contours) around the conserved water site WAT4 at 278 K (upper panels) and 330 K (lower panels) that indicate the proximity of WAT4 to the side chains of Arg8 and Glu13 residues. The contour threshold corresponds to 2.5 times the bulk water density for water oxygens and three times the bulk water density for water hydrogens. The representation of the three helices of the ccβ-p trimer is the same as in Figure 2.

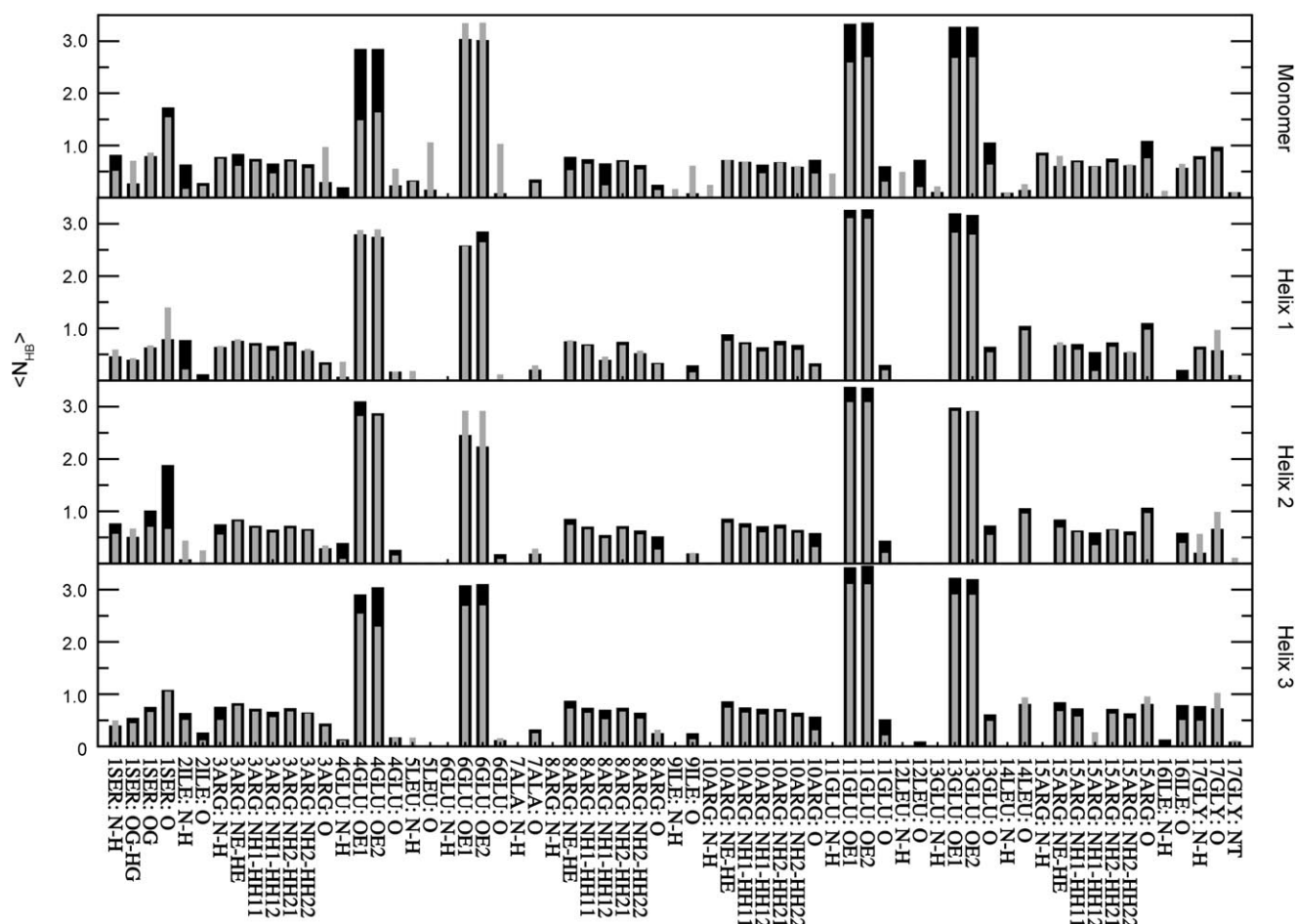


**Figure 4.** Average number of solute-solvent hydrogen bonds ( $\langle N_{\text{HB}} \rangle$ ) per donor or acceptor group for the cc $\beta$ -p monomer and the three helices of the cc $\beta$ -p coiled coil at 278 K (dark) and 330 K (light).

are the Arg residues. Of the seven water sites that were observed in the X-ray data (Table 1), five are proximate to Arg side chains, and four of these are proximate to Glu side chains as well. The average number of hydrogen bonds for a donor/acceptor atom of a Arg residue ranges from 0.12 for the carbonyl oxygen of the Arg8 residue in the cc $\beta$ -p monomer at 330 K to 1.08 for the carbonyl oxygen of the Arg15 residue in helix 1 of the cc $\beta$ -p trimer at 278 K. The overall occurrence of hydrogen bonds between water and the backbone amide hydrogens of all the residues is low. In particular, the amide hydrogens that are buried in the core of the coiled coil do not form hydrogen bonds with the surrounding water.

The average number of hydrogen bonds ( $\langle N_{\text{HB}} \rangle$ ) slightly decreases with increasing temperature from 278 to 330 K. For some residues of the cc $\beta$ -p monomer, the average number of hydrogen bonds increases with temperature, which reflects the pronounced structural differences between the monomers at 278 and 330 K. In the trimer, an increase in the average number of hydrogen bonds at 330 K was observed for the Glu6 side chain of helix 2, which at 330 K becomes more exposed to the surrounding solvent, and for some of the hydrogen-bond donors/acceptors that form the more flexible ends of the cc $\beta$ -p trimer strands.

### Average solvation and water exchange

The average solvation numbers, ( $\langle N_s \rangle$ ), for the backbone carbonyl oxygen and amide hydrogen atoms of the cc $\beta$ -p trimer are shown in Figure 5. In the case of amide hydrogens, the solvation numbers reflect that only the end groups of the coiled coil are exposed to the solvent, whereas amide hydrogens of the interior residues, which are buried in the  $\alpha$ -helices of the coiled coil, are not hydrated. On the other hand, the solvation numbers for the carbonyl oxygen indicates solvation in the interior as well as at the end groups. Consistent with the results of the solute-solvent hydrogen bond analysis, pronounced solvation of the carbonyl oxygen atoms of Arg3, Arg8, Arg10, Glu13, Leu14 and Arg15 residues is observed, whereas the carbonyl oxygen atoms of the remaining residues are less solvated (Ile2, Glu4, Glu6, Ala7, Ile9, Glu11) or not solvated at all (Leu5, Leu12).

The exchange of water molecules in the first hydration shell of the well-solvated carbonyl oxygen atoms is fast and increases with temperature. The rate of exchange events ranges from 0.11 to 5.2 ps $^{-1}$  at 278 K and from 0.09 to 5.5 ps $^{-1}$  at 330 K (see Table S1). Interestingly, the rate of exchange events, ( $\langle N_{\text{exc}} \rangle$ ), correlates very well with the average solvation number (Figure 6)

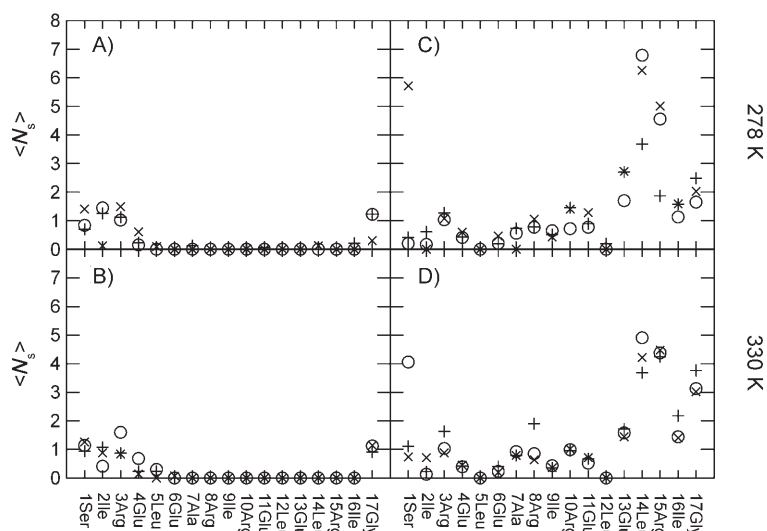


**Figure 5.** Average solvation number  $\langle N_s \rangle$  for the amide hydrogens (panels A and B) and carbonyl oxygens (panels C and D) of the cc $\beta$ -p trimer at 278 and 330 K. The symbols x, o and + designate the three helices of the trimer: o helix 1, x helix 2, + helix 3.

for all residues except Gly17, Arg15, and Glu13 and Leu14; this indicates that the interactions of these residues with water deviate from the average solute–solvent interactions.

#### Residence time distributions

Figure 7 shows the distribution along the backbone of the effective residence times,  $t_{\text{eff}}$ , for water molecules within the first

hydration shell of the backbone atoms of the cc $\beta$ -p trimer, (that is, backbone carbonyl oxygen and amide hydrogen atoms). The values are consistent with both the hydrogen bond and solvation number patterns described above. The residence times at 330 K are expected and found to be systematically lower than at 278 K, due to thermal effects. Of the amide hydrogen atoms, only the residues of the end groups exhibit broad residence time distributions that range between 10 and 40 ps; these show large variations, especially at 278 K, with long residences at Arg3 at 278 K and Leu5 at 330 K, which are likely to be caused by a long visit of a single water molecule in the first hydration shell of the corresponding amide hydrogens. Because such an event can occur only once over the course of the 10 ns simulation periods, the particular residence time is statistically rather unreliable. However, similar deviations are not observed for the backbone carbonyl oxygen atoms, which are generally more exposed to the surrounding solvent; this is consistent with the greater ability

of the surface water molecules to exchange with the bulk phase. The effective residence times that characterise the solvation of carbonyl oxygens show larger variations at 278 K than at 330 K. This is consistent with the above-mentioned enhanced sampling of the configurational space at 330 K. The well-converged pattern of effective residence times at 330 K, which range between 5 and 20 ps, exhibits marginal peaks for Ser1, Arg8 and Glu13. A pronounced hydration of a serine resi-

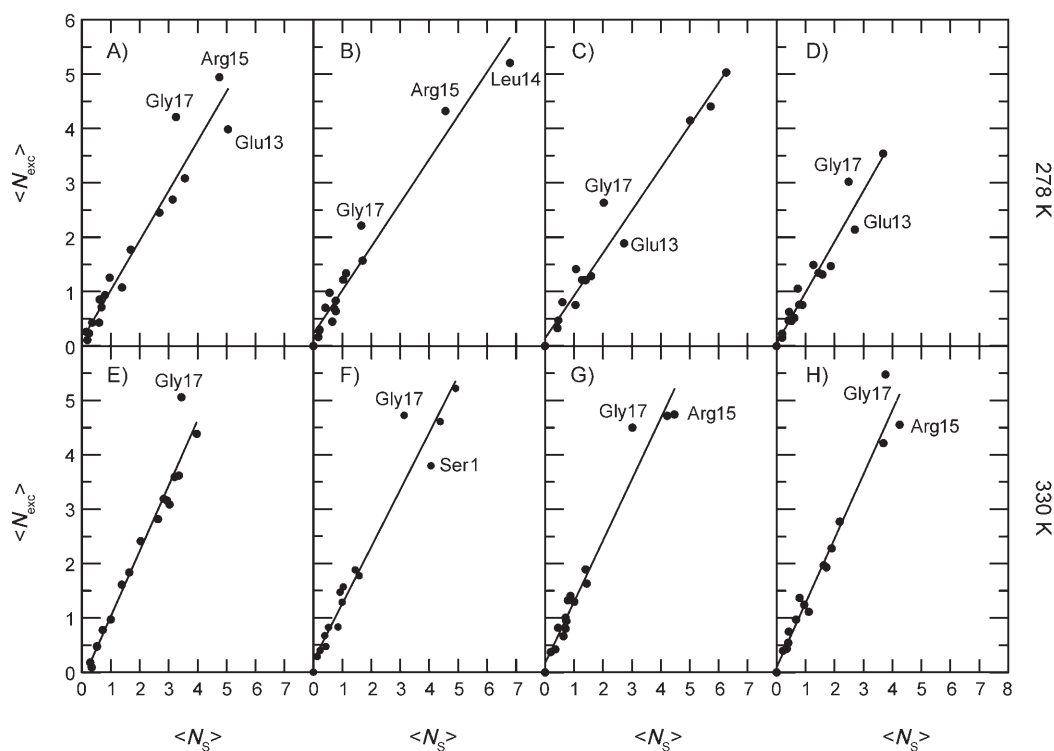


**Figure 6.** Correlation between the average number of water exchanges per ps,  $\langle N_{\text{exc}} \rangle$ , and the average solvation number,  $\langle N_s \rangle$ , for the backbone carbonyl oxygen atoms of the cc $\beta$ -p monomer (panels A and E) and the three helices of the trimer (panels B, C, D, F, G and H) at 278 and 330 K. Outliers are explicitly denoted.

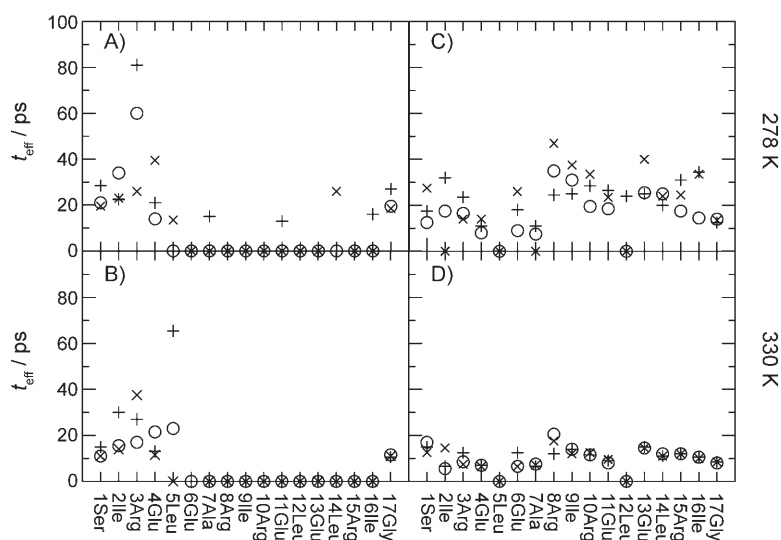


**Figure 7.** Effective residence times  $t_{\text{eff}}$  of water molecules within the first hydration shell of amide hydrogens (panels A and B) and carbonyl oxygens (C and D) of the  $\text{cc}\beta\text{-p}$  trimer at 278 and 330 K. The symbols  $\circ$ ,  $\times$  and  $+$  designate helices 1, 2 and 3, respectively, of the trimer. The time corresponding to the 99th percentile of the residence time distribution was used as effective residence time.

due to its polar side chain is well known,<sup>[41,42]</sup> and the longer effective residence times for the backbone carbonyl oxygen atoms of Arg8 and Glu13 are compatible with the previously reported maxima in the water density distribution and with the position of the crystallographic water site WAT4 that is located between Arg8 and Glu13 residues of the neighbouring chains. However, the correlation between long effective residence times and maxima in the solvent density distribution is weak; prominent maxima do not imply distinctly longer residence times.

The lack of correlation between the spatial and temporal parameters that describe the hydration shell of the  $\text{cc}\beta\text{-p}$  coiled coil is also observed when analysing water residence times within the spherical shells that surround the crystallographic water sites. The maximum residence times for the crystallographic water sites are tabulated in Table 2; the effective residence times range between 1 and 1.5 ps and do not distinguish among these sites. At 278 K, site WAT4, which corresponds to a maximum in the water density distribution ranks at least second among maximum residence times for all helices. At 330 K the maximum water residence times become

**Table 2.** Maximum residence times (in ps) of water molecules within 0.15 nm diameter spherical shells around the crystallographic water sites of helices 1, 2 and 3 of the  $\text{cc}\beta\text{-p}$  coiled coil at 278 and 330 K.

Water site	$t_{\text{max}}$ (helix 1)		$t_{\text{max}}$ (helix 2)		$t_{\text{max}}$ (helix 3)	
	278 K	330 K	278 K	330 K	278 K	330 K
WAT1	3.5	2.0	2.5	2.0	3.5	3.5
WAT2	2.5	2.5	3.0	2.0	3.5	2.5
WAT3	3.0	3.0	5.0	3.5	5.5	3.0
WAT4	5.0	4.0	9.0	4.5	6.0	6.0
WAT5	7.5	3.5	8.0	4.5	6.0	6.0
WAT6	5.0	3.0	4.5	3.0	7.0	3.0
WAT7	3.0	3.0	3.5	2.0	2.5	2.5

shorter due to the thermal effects, and the water sites could not be distinguished based on the water residence time distributions alone.

## Conclusions

By using 10 ns periods of explicit solvent molecular dynamics simulations of the  $\text{cc}\beta\text{-p}$  monomer and coiled coil at 278 and 330 K solvation patterns around the  $\text{cc}\beta\text{-p}$  monomer and  $\text{cc}\beta\text{-p}$  coiled-coil have been identified and compared to the results derived from X-ray crystallography experiments. Analysis of the solvent number density distribution yields well-defined maxima that are compatible with the crystallographic water site that

bridges the neighbouring helices of the coiled coil. The results suggest that the presence of the water molecule between residues Arg8 and Glu13 of the neighbouring helices might make an important contribution to stabilising the trimeric  $\text{cc}\beta\text{-p}$  coiled-coil structure. Analysis of the number density distribution of water hydrogen atoms provided evidence about the orientation of water molecules that correspond to the conserved water site that is beyond crystallographic resolution. Analysis of the residence times of water molecules around the  $\text{cc}\beta\text{-p}$  coiled coil showed that the correlation between the maxima in the solvent number density distribution and the distribution of the residence times of water molecules in the hydration shell of  $\text{cc}\beta\text{-p}$  is weak due to the fast exchange of surface water with bulk water. Nevertheless, water density distributions, hydrogen bonds, solvation numbers, water exchange rates, and effective residence times provide consistent, if not definitive, evidence that the conserved water site is an essential component of the coiled-coil trimerisation motif. The agreement of the simulated results with the experimental data is encouraging, because it shows that MD simulations performed in an explicit solvent can complement experimental data and contribute to understanding the principles of three-stranded coiled-coil formation.

## Experimental Section

**Molecular dynamics simulations:** Four 10 ns long trajectories of previously reported MD simulations<sup>[38]</sup> of the  $\text{cc}\beta\text{-p}$  monomer and the three-stranded  $\alpha$ -helical  $\text{cc}\beta\text{-p}$  coiled coil at 278 and 330 K were submitted to the solvation analysis. Each trajectory was sampled every 0.5 ps, and yielded  $2 \times 10^4$  configurations. The four MD simulations employed the GROMOS96 program modules and the 43A1 force field.<sup>[43–45]</sup> The X-ray structure of  $\text{cc}\beta\text{-p}$  (Protein Data Bank<sup>[46]</sup> ID: 1s9z) supplied the initial coordinates of the peptides in the three-stranded  $\alpha$ -helical coiled-coil trimer configuration.<sup>[34]</sup> The crystallographic asymmetric unit consisted of a  $\text{cc}\beta\text{-p}$  monomer,

seven water oxygens, a Zn and a Na ion. The coordinates for the three-stranded  $\alpha$ -helical coiled coil were generated by using the crystallographic symmetry transformations. All MD simulations of the cc $\beta$ -p monomer and the three-stranded  $\alpha$ -helical cc $\beta$ -p coiled coil reported in this paper were carried out in solution.

For each simulation, the initial configuration placed the solute at the centre of a periodic truncated octahedral box; this required that the minimum distance from any atom of the peptide to the square box walls exceeded 1.4 nm. A cubic periodic array of 216 pre-equilibrated SPC<sup>[47]</sup> water molecules provided the initial configuration of the solvent in the box such that the distance between an oxygen atom of water and nonhydrogen atoms of the solute exceeded 0.23 nm.

Relaxation of the solute–solvent contacts, while positionally restraining the solute atoms by using a harmonic potential energy function with a force constant of 250 kJ mol<sup>-1</sup> nm<sup>-2</sup>, entailed a steepest-descent energy minimisation of the system. A second steepest-descent energy minimisation of the system without restraints followed to eliminate any residual strain; the energy minimisations terminated when the energy change per step became smaller than 0.1 kJ mol<sup>-1</sup>.

Sampling from a Maxwellian distribution at 100 K provided the initial velocities for the MD simulations. Solvent and solute were independently weakly coupled to a temperature bath with a relaxation time of 0.1 ps.<sup>[48]</sup> The systems were also coupled to a pressure bath at 1 atm with a relaxation time of 0.5 ps and an isothermal compressibility of 0.4575  $\times 10^{-3}$  (kJ mol<sup>-1</sup> nm<sup>-3</sup>)<sup>-1</sup>.<sup>[48]</sup> The SHAKE algorithm constrained bond lengths with a geometric tolerance of 10<sup>-4</sup>,<sup>[49]</sup> so that the leapfrog integration time-step could be set to 0.002 ps. Treating the nonbonded interactions employed a triple-range method with cut-off radii 0.8 nm and 1.4 nm.<sup>[50]</sup> Outside the outer cut-off radius, a reaction field with a relative dielectric permittivity of 66.6<sup>[51]</sup> approximated the electrostatic interactions. Within the inner cut-off radius, the evaluation used a charge-group pair list. Short-range interactions entailed updating the list at every time step; interactions between pairs that were separated by distances longer than 0.8 nm and shorter than 1.4 nm entailed updating only every fifth time step.

**Analysis:** The analysed characteristics were solvent number density distributions, hydrogen bonding, solvent accessibility, water exchange events and residence times.

The solvent number density distributions were obtained by placing the initial solute configuration at the centre of a three-dimensional cubic grid with a 0.05 nm grid step as a reference frame. The rotational least-squares fit<sup>[52,53]</sup> of the protein backbone atoms C $\alpha$ , N and C onto the reference frame removed the effects of centre-of-mass translations or solute rotations. The three-dimensional water density distribution was calculated by averaging the number of oxygen atoms in each grid cell over the entire trajectory.<sup>[23,27,54]</sup> Hydration sites were defined as maxima in the water density distribution that had a density no lower than two times the value of bulk water. A water density of 1 g cm<sup>-3</sup> corresponded to an oxygen number density of 33.5 nm<sup>-3</sup>.

Solvent-accessible surface area (SASA) values for individual cc $\beta$ -p structures were calculated by using the program NACCESS<sup>[55,56]</sup> by using a probe with a radius of 0.14 nm.

Hydrogen bonds between cc $\beta$ -p and water were defined by the following geometric criterion: the hydrogen–acceptor distance must be less than or equal to 0.25 nm and the donor–proton–acceptor angle at least 135°. Because the hydration of cc $\beta$ -p is a

highly dynamic process, each cc $\beta$ -p donor or acceptor atom formed hydrogen bonds with many different water molecules. Thus, the average number of hydrogen bonds  $\langle N_{\text{HB}} \rangle$  of a cc $\beta$ -p donor/acceptor atom with the surrounding water molecules was calculated as a sum over the average number of hydrogen bonds the donor/acceptor atom forms with each of the water molecules in the simulation box [Eq. (1)]:

$$\langle N_{\text{HB}} \rangle = \frac{1}{N_{\text{C}}} \sum_{j=1}^{N_{\text{W}}} N_{\text{HB},\text{Wj}} \quad (1)$$

where  $N_{\text{HB},\text{Wj}}$  is the number of hydrogen bonds a donor or acceptor group forms with the water molecule Wj,  $N_{\text{C}}$  is the number of configurations analysed and  $N_{\text{W}}$  is the number of water molecules in the simulation box. Because of the possible occurrence of three-centre hydrogen bonds, the average number of hydrogen bonds per donor or acceptor group of the cc $\beta$ -p can exceed one.

To gain insight into the solvation of the cc $\beta$ -p monomer and coiled coil, the average solvation numbers and number of exchange events as well as the average, maximal and effective residence time of water molecules were calculated for the carbonyl oxygen and amide hydrogen atoms of the cc $\beta$ -p backbone. Moreover, residence times were also calculated for the water molecules in spherical shells that surrounded the crystallographic water sites. The hydration shell radii,  $r_{\text{sh}}$ , of a solute atom was defined as [Eq. (2)]:

$$r_{\text{sh}} = r_{\text{ex}} + \Delta r_{\text{RT}} \quad (2)$$

where  $r_{\text{ex}}$  is the first minimum of the radial pair distribution function for the solute atom and the oxygen atom of water and  $\Delta r_{\text{RT}} = 0.05$  nm accounts for positional fluctuations.<sup>[21]</sup> Analysis of the crystallographic water sites was performed by monitoring the exchange of water molecules within the 0.15 nm diameter spherical shells that were constructed around the positions of the water oxygen atoms as determined by X-ray crystallography. With the definition of the spherical shells, the average solvation number, number of exchange events, average and maximal residence times could be deduced directly from the simulated trajectories. However, these times are not experimentally accessible, and a fit of the temporal autocorrelation function to a single exponential<sup>[21]</sup> served to define an observable effective residence time. Several authors have observed that the temporal autocorrelation function from MD simulations cannot be approximated by a single exponential function very well.<sup>[27,30,57,58]</sup> Our simulations confirmed the nonexponential behaviour of this autocorrelation function, and we decided to choose as an effective residence time the time that defined the 99th percentile of the cumulative distribution of residence times, that is, 1% of the water residencies lasted longer than the effective residence time.

## Acknowledgement

Financial support by the National Centre of Competence in Research (NCCR) (Structural Biology) of the Swiss National Science Foundation (SNSF) and by the Slovenian Research Agency (ARRS) is gratefully acknowledged. In addition, J.D. would like to thank U. Borštnik and V. Kräutler for valuable discussions and suggestions.

**Keywords:** coiled coil • crystallographic water • molecular dynamics • solvent effects • surface hydration

- [1] M. Levitt, B. H. Park, *Structure* **1993**, *1*, 223–226.
- [2] S. K. Pal, A. H. Zewail, *Chem. Rev.* **2004**, *104*, 2099–2123.
- [3] V. Helms, *ChemPhysChem* **2007**, *8*, 23–33.
- [4] J. A. Ernst, R. T. Clubb, H. X. Zhou, A. M. Gronenborn, G. M. Clore, *Science* **1995**, *267*, 1813–1817.
- [5] V. P. Denisov, B. Halle, *Faraday Discuss.* **1996**, 227–244.
- [6] R. Baron, J. A. McCammon, *Biochemistry* **2007**, *46*, 10629–10642.
- [7] D. I. Svergun, S. Richard, M. H. J. Koch, Z. Sayers, S. Kuprin, G. Zaccai, *Proc. Natl. Acad. Sci. USA* **1998**, *95*, 2267–2272.
- [8] C. A. Schiffer, W. F. van Gunsteren, *Proteins: Struct., Funct., Genet.* **1999**, *36*, 501–511.
- [9] M. Tarek, D. J. Tobias, *Biophys. J.* **2000**, *79*, 3244–3257.
- [10] D. M. Leitner, M. Havenith, M. Gruebele, *Int. Rev. Phys. Chem.* **2006**, *25*, 553–582.
- [11] L. W. Yang, E. Eyal, C. Chennubhotla, J. Jee, A. M. Gronenborn, I. Bahar, *Structure* **2007**, *15*, 741–749.
- [12] G. Otting, E. Liepinsh, K. Wüthrich, *J. Am. Chem. Soc.* **1992**, *114*, 7093–7095.
- [13] G. Melacini, A. Bonvin, M. Goodman, R. Boelens, R. Kaptein, *J. Mol. Biol.* **2000**, *300*, 1041–1048.
- [14] M. Marchi, F. Sterpone, M. Ceccarelli, *J. Am. Chem. Soc.* **2002**, *124*, 6787–6791.
- [15] K. Modig, E. Liepinsh, G. Otting, B. Halle, *J. Am. Chem. Soc.* **2004**, *126*, 102–114.
- [16] X. Daura, I. Antes, W. F. van Gunsteren, W. Thiel, A. E. Mark, *Proteins: Struct. Funct. Genet.* **1999**, *36*, 542–555.
- [17] B. Zagrovic, V. S. Pande, *Biophys. J.* **2004**, *87*, 2240–2246.
- [18] W. F. van Gunsteren, D. Bakowies, R. Baron, I. Chandrasekhar, M. Christen, X. Daura, P. Gee, D. P. Geerke, A. Glättli, P. H. Hünenberger, M. A. Kastenholz, C. Ostenbrink, M. Schenk, D. Trzesniak, N. F. A. van der Vegt, H. B. Yu, *Angew. Chem.* **2006**, *118*, 4168–4198; *Angew. Chem. Int. Ed.* **2006**, *45*, 4064–4092.
- [19] W. F. van Gunsteren, H. J. C. Berendsen, J. Hermans, W. G. J. Hol, J. P. M. Postma, *Proc. Natl. Acad. Sci. USA* **1983**, *80*, 4315–4319.
- [20] M. Feig, B. M. Pettitt, *Structure* **1998**, *6*, 1351–1354.
- [21] R. M. Brunne, E. Liepinsh, G. Otting, K. Wüthrich, W. F. van Gunsteren, *J. Mol. Biol.* **1993**, *231*, 1040–1048.
- [22] P. J. Steinbach, B. R. Brooks, *Proc. Natl. Acad. Sci. USA* **1993**, *90*, 9135–9139.
- [23] V. Lounnas, B. M. Pettitt, *Proteins: Struct., Funct., Genet.* **1994**, *18*, 148–160.
- [24] G. Hummer, A. E. Garcia, D. M. Soumpasis, *Biophys. J.* **1995**, *68*, 1639–1652.
- [25] A. Bonvin, M. Sunnerhagen, G. Otting, W. F. van Gunsteren, *J. Mol. Biol.* **1998**, *282*, 859–873.
- [26] A. E. Garcia, G. Hummer, *Proteins: Struct., Funct., Genet.* **2000**, *38*, 261–272.
- [27] V. A. Makarov, B. K. Andrews, P. E. Smith, B. M. Pettitt, *Biophys. J.* **2000**, *79*, 2966–2974.
- [28] D. Bakowies, W. F. van Gunsteren, *J. Mol. Biol.* **2002**, *315*, 713–736.
- [29] D. Bakowies, W. F. van Gunsteren, *Proteins: Struct., Funct., Genet.* **2002**, *47*, 534–545.
- [30] A. R. Bizzarri, S. Cannistraro, *J. Phys. Chem. B* **2002**, *106*, 6617–6633.
- [31] F. Merzel, J. C. Smith, *Proc. Natl. Acad. Sci. USA* **2002**, *99*, 5378–5383.
- [32] A. De Simone, G. G. Dodson, C. S. Verma, A. Zagari, F. Fraternali, *Proc. Natl. Acad. Sci. USA* **2005**, *102*, 7535–7540.
- [33] A. De Simone, R. Spadaccini, P. A. Temussi, F. Fraternali, *Biophys. J.* **2006**, *90*, 3052–3061.
- [34] R. A. Kammerer, D. Kostrewa, J. Zurdo, A. Detken, C. Garcia-Echeverria, J. D. Green, S. A. Muller, B. H. Meier, F. K. Winkler, C. M. Dobson, M. O. Steinmetz, *Proc. Natl. Acad. Sci. USA* **2004**, *101*, 4435–4440.
- [35] M. O. Steinmetz, C. Garcia-Echeverria, R. A. Kammerer, *Int. J. Peptide Res. Therapeut.* **2005**, *11*, 43–52.
- [36] R. A. Kammerer, M. O. Steinmetz, *J. Struct. Biol.* **2006**, *155*, 146–153.
- [37] R. A. Kammerer, D. Kostrewa, P. Progiass, S. Honnappa, D. Avila, A. Lustig, F. K. Winkler, J. Pieters, M. O. Steinmetz, *Proc. Natl. Acad. Sci. USA* **2005**, *102*, 13891–13896.
- [38] J. H. Missimer, M. O. Steinmetz, R. Baron, F. K. Winkler, R. A. Kammerer, X. Daura, W. F. van Gunsteren, *Protein Sci.* **2007**, *16*, 1349–1359.
- [39] P. I. W. de Bakker, P. H. Hünenberger, J. A. McCammon, *J. Mol. Biol.* **1999**, *285*, 1811–1830.
- [40] R. H. Henchman, J. A. McCammon, *J. Comput. Chem.* **2002**, *23*, 861–869.
- [41] S. R. Trevino, J. M. Scholtz, C. N. Pace, *J. Mol. Biol.* **2007**, *366*, 449–460.
- [42] J. Chang, A. M. Lenhoff, S. I. Sandler, *J. Phys. Chem. B* **2007**, *111*, 2098–2106.
- [43] W. F. van Gunsteren, S. R. Billeter, A. A. Eising, P. H. Hünenberger, P. Krüger, A. E. Mark, W. R. P. Scott, I. G. Tironi, *Biomolecular Simulation: The GROMOS96 Manual and User Guide*, Vdf Hochschulverlag, Zürich, **1996**.
- [44] W. R. P. Scott, P. H. Hünenberger, I. G. Tironi, A. E. Mark, S. R. Billeter, J. Fennen, A. E. Torda, P. Huber, P. Krüger, W. F. van Gunsteren, *J. Phys. Chem. A* **1999**, *103*, 3596–3607.
- [45] X. Daura, A. E. Mark, W. F. van Gunsteren, *J. Comput. Chem.* **1998**, *19*, 535–547.
- [46] H. M. Berman, J. Westbrook, Z. Feng, G. Gilliland, T. N. Bhat, H. Weissig, I. N. Shindyalov, P. E. Bourne, *Nucleic Acids Res.* **2000**, *28*, 235–242.
- [47] H. J. C. Berendsen, J. P. M. Postma, W. F. van Gunsteren, J. Hermans in *Intermolecular Forces* (Ed.: B. Pullman), Reidel, Dordrecht, **1981**, pp. 331–342.
- [48] H. J. C. Berendsen, J. P. M. Postma, W. F. van Gunsteren, A. Dinola, J. R. Haak, *J. Chem. Phys.* **1984**, *81*, 3684–3690.
- [49] J.-P. Ryckaert, G. Ciccotti, H. J. C. Berendsen, *J. Comput. Phys.* **1977**, *23*, 327–341.
- [50] W. F. van Gunsteren, H. J. C. Berendsen, *Angew. Chem.* **1990**, *102*, 1020–1055; *Angew. Chem. Int. Ed. Engl.* **1990**, *29*, 992–1023.
- [51] I. G. Tironi, R. Sperb, P. E. Smith, W. F. van Gunsteren, *J. Chem. Phys.* **1995**, *102*, 5451–5459.
- [52] A. D. McLachlan, *J. Mol. Biol.* **1979**, *128*, 49–79.
- [53] S. K. Kearsley, *Acta Crystallogr. Sect. A* **1989**, *45*, 208–210.
- [54] V. Lounnas, B. M. Pettitt, *Proteins: Struct., Funct., Genet.* **1994**, *18*, 133–147.
- [55] S. J. Hubbard, J. M. Thornton: *NACCESS, Computer program*, University College London, **1993**.
- [56] B. Lee, F. M. Richards, *J. Mol. Biol.* **1971**, *55*, 379–400.
- [57] C. Rocchi, A. R. Bizzarri, S. Cannistraro, *Chem. Phys.* **1997**, *214*, 261–276.
- [58] V. A. Makarov, B. M. Pettitt, M. Feig, *Acc. Chem. Res.* **2002**, *35*, 376–384.

Received: February 13, 2008

Published online on June 13, 2008